Radiation therapy promotes unsaturated fatty acids to maintain survival of glioblastoma

Mara De Martino[1], Camille Daviaud[1], Hanna E. Minns[2], Nabeel Attarwala[3], Qiuying Chen[3], Noah Dephoure[4, 5], Robyn D. Gartrell[2], Evagelia C. Laiakis[6] and Claire Vanpouille-Box[1, 5*].

[1]Department of Radiation Oncology, Weill Cornell Medicine, New York, NY, USA. [2]Department of Pediatrics, Pediatrics Hematology/Oncology/Stem Cell Transplant, Columbia University Irving Medical Center, New York, NY, USA. [3]Department of Pharmacology, Weill Cornell Medicine, New York, NY, USA. [4]Department of Biochemistry, Weill Cornell Medicine, New York, USA. [5]Sandra and Edward Meyer Cancer Center, New York, NY, USA. [6]Department of Oncology, Georgetown University, Washington, DC, USA.

Running title: RT augments lipid metabolism in glioblastoma

Keywords: Radiation therapy, glioblastoma, lipid metabolism, unsaturated fatty acids, survival.

***Corresponding author:** Claire Vanpouille-Box, Department of Radiation Oncology, Weill Cornell Medicine, New York, NY, USA. E-mail: clv2002@med.cornell.edu; Phone: 646-962-2125; Fax: 212-746-7815.

Conflict of interest statement: The authors declared that no conflict of interest exists related to this work.

Funding statement: This work was supported by Vanpouille-Box Lab start-up funds from the Department of Radiation Oncology at Weill Cornell Medicine (New York, NY). C.V-B. Lab is further supported by the Uncle Kory Seed Grant from the Uncle Kory Foundation.

Data sharing statement: Some data generated in this study are available within the article and its supplementary data files. Other data generated in this study are available upon request from the corresponding author.

Acknowledgments: We are acknowledging the Weill Cornell Medicine Proteomics and Metabolomics Core Facility for their assistance in profiling free fatty acids in irradiated murine glioblastoma cells. We are grateful to the Electron Microscopy & Histology services of the Weill Cornell Medicine Microscopy & Image Analysis Core for their assistance in transmission electronic images.

ABSTRACT (300 words)

Purpose: Radiation therapy (RT) is essential for the management of glioblastoma (GBM) and is the only effective treatment for inoperable brain tumors. However, GBM frequently relapses within the irradiated margins, thus suggesting that RT might stimulate mechanisms of resistance that limits its efficacy. GBM is recognized for its metabolic plasticity, but whether RT-induced resistance relies on metabolic adaptation remains unclear.

Methods and Materials: We analyzed *in vitro* extracellular flux and profiled targeted metabolites as well as free fatty acids in two syngenic models of glioblastomas 24hrs post RT. Metabolic adaptation of irradiated GBM were confirmed *in vivo* by mass spectrometry imaging five days post RT. The role of the fatty acid synthase (FASN) in RT-induced lipid metabolites was assessed by genetical and pharmacological inhibition of *Fasn* in irradiated GBM cells. The impact of FASN-mediated lipids on endoplasmic reticulum (ER) stress and apoptosis of irradiated GBM cells were performed by transmission electronic microscopy, western blot and flow cytometry 24hrs post RT. Analysis of a public dataset of GBM patients was performed to correlate preclinical findings.

Results: Here, we show *in vitro* and *in vivo* that irradiated GBM tumors switch their metabolic program to accumulate lipids, especially unsaturated fatty acids. This resulted in an increase formation of lipid droplets to prevent ER stress. We uncovered that FASN is critical for lipid accumulation of irradiated GBM and demonstrate that genetic suppression of *Fasn* leads to mitochondrial dysfunction and apoptosis. Supporting the translational value of these findings, retrospective analysis of a public dataset of GBM patients revealed an enrichment in lipid metabolism and fatty acid biosynthesis signatures in recurrent GBM compared to primary.

Conclusions: Overall, these results demonstrate that RT drives GBM resistance by generating a lipogenic environment permissive to GBM survival. Targeting lipid metabolism might be required to develop more effective anti-GBM strategies.

INTRODUCTION

Glioblastoma (GBM) is the most aggressive primary brain cancer in adults and accounts for 3-15% of central nervous system (CNS) tumors in children. A rising incidence of GBM has been observed over the last 15 years (1,2), while the median survival of GBM patients remains unchanged (15 months); consequently, GBM mortality is predicted to increase. Radiation therapy (RT) is the standard-of-care for the management of GBM (3,4) and is the only effective treatment for inoperable brain tumors (5,6). Unfortunately, GBM recurrence often arises within the irradiated margins (7), suggesting that RT might not optimally control GBM and might generate and/or exacerbate resistance mechanisms to support GBM progression. The mechanisms by which RT drives evasion of GBM are unknown.

GBM is recognized for its altered tumor metabolism and for its ability to respond to metabolic stressors during cancer progression and treatment (8). For instance, GBM cells can metabolize glucose into lactate irrespective of the presence of oxygen to use glucose-derived carbons for the synthesis of essential cellular components, while generating enough ATP to support cellular processes (9). Consequently, while GBM (like many other tumors) relies on glycolysis as energy supply, it possesses the flexibility to switch metabolic programs in order to adapt to the heterogeneity of its tumor microenvironment (TME) which includes distinct regions of hypoxia, necrosis, angiogenesis and different availabilities of nutrients (10). In that context, other metabolic pathways such as glutamine and lipid metabolism are actively investigated as alternative energy sources to identify additional metabolic liabilities for anti-GBM therapies (11,12).

Oxidative stressors, like reactive oxygen species (ROS) generated by RT, have been shown to reprogram the metabolism of an irradiated tumor (11,13). Such metabolic reprogramming, in part, can promote the aggressivity of GBM. One study reported that a 20 Gy irradiation of healthy

mouse brains prior to orthotopic implantation of human GBM cells worsens GBM outcome due to enhanced tumor cell proliferation and migration, as well as microglial activation (14). While increased levels of ATP and GTP with reduced levels of antioxidants, glutathione and ascorbate, were associated with the poor outcome of GBM in pre-irradiated brains (14), a comprehensive identification of the metabolic pathways altered in irradiated GBM tumors as well as their consequences for GBM growth and resistance is underexplored.

Here, we define the metabolic switch of GBM in response to RT *in vitro* and *in vivo*, uncovering the role of unsaturated fatty acids (UFAs) in providing metabolic plasticity of GBM; thereby allowing GBM cells to adapt to genotoxic stress and develop resistance mechanisms. This includes serving as a metabolic cue to prevent endoplasmic reticulum (ER) stress and resistance to apoptosis, while serving as an additional energy supply to permit survival of GBM. Specifically, our data demonstrate that accumulation of UFAs post RT leads to the formation of lipid droplet, a major site for the synthesis of the bioactive lipid prostaglandin E2 (PGE2) that is ascribed roles in cancer stemness and immunossupression. Analysis of the public HG-UG133A dataset of GBM patients from The Cancer Genome Atlas (TCGA) revealed an increased expression of lipid metabolism signatures as well as an enrichment of fatty acid biosynthesis in recurrent GBM compared to primary and confirms the upregulation of prostaglandins in recurrent GBM patients. Thus, supporting the clinical relevance of this regulatory mechanism.

Consequently, these observations indicate that RT induces a growth permissive metabolic reprogramming by increasing tumor-derived UFAs in GBM, suggesting that targeting lipid metabolism in the context of RT may be required to prevent GBM recurrence.

METHODS

Mice

Eight-week-old C57BL/6N female mice from Taconic Animal Laboratory (Germantown, NY) were maintained under pathogen-free conditions in the animal facility at Weill Cornell Medicine. All experiments were approved by the Institutional Animal Care and Use Committee.

Cells and reagents

C57BL/6N mouse-derived GBM GL261 were obtained from S. Demaria (15) and CT2A were purchased from Millipore-Sigma (Burlington, MA). GL261 and CT2A are poorly immunogenic and share the growth characteristics as well as invasive properties of human GBM. Intracerebral (i.c.) injection of $5x10^4$ GL261 or CT2A cells into syngeneic C57BL/6N results in the death of the mice in approximately 20-25 days (15,16). U118 human GBM cells were purchased from ATCC (Manassas, VA). All cells were authenticated by IDEEX Bioresearch (Columbia, MO), and further characterized by morphology, phenotype, growth and pattern of metastasis *in vivo* and routinely screened for *Mycoplasma* (LookOut® Mycoplasma PCR Detection kit, Sigma-Aldrich). None of the cells used are listed in the International Cell Line Authentication Committee (ICLAC) database of commonly misidentified cell lines. GL261, CT2A and U118 were cultured in DMEM (GIBCO) supplemented with 2 mmol/L L-glutamine, 100 U/mL penicillin, 100 µg/mL streptomycin, 2.5×10^{-5} mol/L 2-mercapthoethanol, and 10% fetal bovine serum (FBS) (Life technologies). For experiments with doxycycline, cells were grown in media containing tetracycline-FBS and induced with 4µg/mL of doxycycline 10 days prior to treatment.

shRNA-mediated gene knock-down and lentiviral transduction

HEK 293-FT cells were used to produce viruses upon transfection of the packaging plasmids pPAX2 and pMD2 and a pTRIPZ vector containing a tetracycline-inducible promoter (GE

Dharmacon technology, kindly provided by Dr. Robert Schneider). ShRNAs directed against FASN mRNA (*Fasn*, mouse-shRNA: GACAGCGCATGCCTTTGTAAAC) or a non-silencing sequence (NS; mouse-human-shRNA: AATTCTCCGAACGTGTCACGT) were cloned into pTRIPZ using EcoRI and XhoI restriction sites. GL261 and CT2A cells were transduced with cell-free virus-containing supernatants and selected with 4μg/mL of puromycin for 48 hours.

CRISPR/Cas9

To generate Fasn-deficient clones using CRISPR, GL261 and CT2A cells were transduced with lentiviral particles, to incorporate a lentiviral vector containing guide RNA (gRNA) and Cas9 coexpression (VectorBuilder, IL). Two *Fasn* targeting ccRNA were used (#1: pLV[CRISPR]-hCas9:T2A:Puro-U6>mFasn[gRNA#1485], ccRNA: GATGAACGTGTACCGGGACG; #2: pLV[CRISPR]-hCas9:T2A:Puro-U6>mFasn[gRNA#2246], ccRNA: CACGGCCGCGCTCGGCTCGA), and a scramble ccRNA (pLV[CRISPR]-hCas9:T2A:Puro-U6>Scramble[gRNA#1], ccRNA: GTGTAGTTCGACCATTCGTG). After lentiviral transduction, cells underwent puromycin selection (4μg/mL) and were single-cell plated into 96 well plates, and allowed to grow for at least 2 weeks. Resulting FASN-deficient clones were screened by western blot.

Extracellular Flux Analysis

Cellular respiration (oxygen consumption rate (OCR) and extracellular acidification (ECAR)) were assessed using the XF96 Extracellular Analyzer as described in manufacturer's instructions for the XF cell mito stress and the XF cell mito fuel flex test kits (Agilent Technologies, CA).Briefly, $1.5x10^6$ GL261 or CT2A cells were plated in a 10-cm dish on day 0. Fourty eight hours after plating, cells received a radiation dose of 0 Gy or 10 Gy using the Small Animal Radiation Research Platform (SARRP, Xstrahl Inc, Suwanee GA; open field, 2.82 Gy/min). Immediately

after irradiation, $4x10^4$ cells/well were seeded in the XF Cell Culture Microplate and incubated for 24 hours at 37°C. The following day, cells were incubated with 180 μl of Seahorse XF DMEM supplemented with 2 mM L-glutamine, 1 mM sodium pyruvate, and 10 mM glucose for 1 hour prior to assay. The XF Mito Stress Test kit was used to measure mitochondrial respiration as described by the manufacturer. The OCR was measured with sequential injection of 1 μM oligomycin A, 1 μM carbonilcyanide *p*-triflouromethoxyphenylhydrazone (FCCP), and 0.5 μM rotenone/antimycinA. The Seahorse XF Mito Fuel Test kit was also used to measure the mitochondrial fuel usage in live cells. The OCR was measured after injection of 3 μM BPTES (glutamine oxidation inhibitor), 4 μM etomoxir(fatty acid oxidation inhibitor), or 2 μM UK5099 (glycolysis inhibitor). Each inhibitor was injected in a different order to determine the cell dependence on each fuel oxidation pathway. After retrieving the plate from Seahorse instrument, live cell nuclei were stained with NucRed™ Live 647 ReadyProbes™ Reagent (Thermo Fisher Scientific) as per the manufacturer's instruction. Whole well images were obtained by Spectramax i3x and live cell nuclei were counted (Molecular Devices Jose, CA). All measurements were normalized to the number of live cells in each well and were performed in two biological replicates with 6-12 technical replicates per group.

Targeted Profiling of Polar Metabolites

$1.5x10^6$ GL261 cells were plated in a 10-cm dish on day 0. Twenty four hours after incubation, cells received a radiation dose escalation from 0 Gy, 6 Gy and 10 Gy (n=3 per condition) using the SARRP (open field, 2.82 Gy/min). Immediately after irradiation, medium was replaced in each dish, including the control. Twenty four hours after irradiation, cells were washed twice with cold PBS.The liquid was removed from the dish as thoroughly as possible. The dish was then placed on dry ice. One mL of cold 80% methanol was added to the 10-cm dish prior to cell scraping. Lysates were then transferred into a cold microcentrifuge tube, vortexed 1 min, left on dry ice for 5 min and vortexed 1 min again. Next, lysates were centrifuged at 14,000 x g for 20 min at 4°C.

Lysates were then transferred to a 1.5mL cold microcentrifuge tube and stored at -80°C until mass spectrometry analysis at the Weill Cornell Medicine Proteomics and Metabolomics Core Facility. Polar metabolite targeted profiling was performed according to a method described in a previous publication (17). Metabolites were extracted from cells using pre-chilled 80% methanol (-80 °C). The extract was dried completely with a Speedvac (no heat). The dried sample was redissolved in HPLC grade water before it was analyzed with hydrophilic interaction liquid chromatography (HILC) mass spectrometry (MS). Metabolites were measured on a Vanquish UPLC system (ThemoScientific) via an Ion Max ion source with HESI II probe (Thermo Scientific), coupled to a Q Exactive Orbitrap mass spectrometer (Thermo Scientific). A Sequant ZIC-pHILIC column (2.1 mm i.d. × 150 mm, particle size of 5 µm, Millipore Sigma) was used for separation of metabolites. A 2.1 × 20 mm heated guard column with the same packing material was used for protection of the analytical column. Flow rate was set at 150 µL/min. Buffers consisted of 100% acetonitrile for mobile phase A, and 0.1% NH_4OH/20 mM CH_3COONH_4 in water for mobile phase B. The chromatographic gradient ran from 85% to 30% A in 20 min followed by a wash with 30% A and re-equilibration at 85% A. The Q Exactive was operated in full scan, polarity-switching mode with the following parameters: the spray voltage 3.0 kV, the heated capillary temperature 300 °C, the HESI probe temperature 350 °C, the sheath gas flow 40 units, the auxiliary gas flow 15 units. MS data acquisition was performed in the *m/z* range of 70–1,000, with 70,000 resolution (at 200 *m/z*). The AGC target was 1e6 and the maximum injection time was 250 ms. The MS data was processed using XCalibur 4.1 (Thermo Scientific) to obtain signal intensity of each metabolite for relative quantification. Metabolites were identified using an in-house library established using chemical standards. Identification required accurate mass (within 5ppm) and standard retention times. The intensity values were normalized to total cell count prior downstream analysis.

Free Fatty Acid Profiling

$1.5x10^6$ GL261 or CT2A cells were plated in a 10-cm dish on day 0. Twenty four hours after plating, cells received a radiation dose escalation from 0 Gy, 6 Gy and 10 Gy (n=5 per condition) using the SARRP (open field, 2.82 Gy/min). Immediately after irradiation, medium was replaced in each dish, including the control. Twenty four hours after irradiation, cells were detached from plates with trypsin, washed twice with cold PBS and spun down for 5 min at 340xg. Cells were then transferred to a 1.5mL centrifuge tube and stored at -80°C until mass spectrometry analysis at the Weill Cornell Medicine Proteomics and Metabolomics Core Facility.

Briefly, free fatty acids were extracted from cells using 90% methanol (LC-MS grade, Thermo Scientific). The extracts were clarified by centrifugation at 15,000 x g for 10 min. The supernatant was collected and dried down using a SpeedVac. The dried sample was reconstituted using 50% methanol prior to LC-MS analysis.

Chromatographic separation was performed on a Vanquish UHPLC system (Thermo Scientific) with a Cadenza CD-C18 3 µm packing column (Imtakt, 2.1 mm id x 150 mm) coupled to a Q Exactive Orbitrap mass spectrometer (Thermo Scientific) via an Ion Max ion source with a HESI II probe (Thermo Scientific). The mobile phase consisted of buffer A: 5 mM ammonium acetate in water (LC-MS grade, Thermo Scientific) and buffer B: 5 mM ammonium acetate, 85% isopropanol (LC-MS grade, Thermo Scientific), 10% acetonitrile (LC-MS grade, Thermo Scientific), and 5% water. The LC gradient was as follows: 0–1.5 min, 50% buffer B; 1.5-3 min, 50-90% buffer B; 3-5.5 min, 90-95% buffer B; 5.5-10 min, 95% buffer B, followed by 5 min of re-equilibration of the column before the next run. The flow rate was 150 µL/min. MS data was acquired in negative ionization mode. The following electrospray parameters were used: spray voltage 3.0 kV, heated capillary temperature 350 °C, HESI probe temperature 350 °C,sheath gas, 35 units; auxiliary gas 10 units. For MS scans: mass scan range, 140-1000 *m/z*; resolution, 70,000 (at *m/z* 200); automatic gain control target, 1e6; maximum injection time, 50 ms.

MS data files were processed using XCalibur (version 4.1, Thermo Scientific). Identification of free fatty acids was based on accurate masses within 5 ppm and standard retention times from compound standards. Relative quantitation was performed based on MS signal intensities. The intensity values were normalized by the total protein in each sample (determined by the Pierce™ BCA Protein assay kit, ThermoFisher Scientific, cat# 23225) before they were used for quantitative analysis.

Targeted Profiling of Polar Metabolites and Free Fatty Acid Profiling Analysis

Statistical analysis was performed with the online software MetaboAnalyst 5.0 (18). Analysis of polar metabolites was constricted to metabolites that were common between the two independent experiments of GL261. Data were not transformed, but were Pareto scaled for both sets of analyses. Statistical analysis was performed with an ANOVA with an adjusted p-value (false discovery rate FDR) cutoff of <0.05 and Tukey's as the post-hoc analysis. Fatty acid analysis was based on the comparison between GL261 and CT2A on the statistically significant metabolites. Data were visualized in the form of a principal component analysis (PCA) scores plot based on the first two components and in heatmaps with Euclidean distance measure and Ward clustering. Enrichment analysis of the polar metabolites was KEGG pathway based and only metabolite sets that contained at least 5 entries were used.

Tumor Challenge and Treatment

On day 0, tumor cells (i.e. GL261 or CT2A) for intracerebral implantation were trypsinized, counted and checked for viability by trypan blue exclusion. Cells were washed twice with DMEM without FBS or antibiotics, and a final suspension of $25x10^6$ cells/mL in DMEM was prepared. Mice were anesthesized with 1.5% isoflurane. Using a stereotactic head frame and a 5μL Hamilton syringe (Hamilton glass syringe 700 series RN), $5x10^4$ in 2μL of GL261 or CT2A cells

were injected into the mice right striatum. The coordinates used for intracerebral injection were 0.5mm anterior to the bregma, 2mm lateral to the saggital suture (right hemisphere), and 3 mm below the dura. Mice with established GL261 and CT2A tumors were selectively irradiated with 0Gy or 10Gy ten days after tumor cells implantation as previously described (19). Briefly, mice were anesthetized with isoflurane to perform computed tomographic (CT) imaging on the SARRP to identify the burr hole from tumor implantation, which was used to aim 10Gy-radiation in a 3mm beam centered on the tumor. The dose rate was 2.39Gy/min.

Matrix-Assisted Laser Desoprtion Ionization Imaging Mass Spectrometry (MALDI-IMS)

Brains from tumor-bearing animals were frozen at day 15 (i.e. 5 days after irradiation) in isopentane cooled with dry ice and stored at -80°C. Ten micron cryosections from 3 brains per group were mounted on conductive slides coated with Indium Tin Oxide (ITO) (Delta Technologies; cat # CB-90IN-S111) to perform MALDI-IMS using the Bruker SciMax in an ultra-high mass resolution Fourier Transform – Ion Cyclotron Resonance (FT-ICR) mass spectrometer. Briefly, ITO-slides with tissue sections are transferred from -80°C to a vacuum chamber and dried for 30 min prior to matrix deposition using N-(1-naphthyl) ethylenediamine dihydrochloride (NEDC, 10mg ml^{-1} in 75% methanol) for negative ion detection and 2,5-Dihydroxybenzoic acid (DHB, 30mg/ml in 90% acetonitrile) for positive ion detection, using a matrix sprayer HTX TM-Sprayer™ (HTX Technologies LLC, NC). Matrix-coated tissue sections are dried in vacuum desiccator for 20min before loading for MALDI-IMS data acquisition on a 7T Scimax-MRMS mass spectrometer (Bruker Daltonics, USA) equipped with a SmartBeam II laser and a MALDI source (spatial resolution set at 80μm). Acquired image data were exported to Scils Lab software (SCiLS, Bremen, Germany) and Cardinal R package (https://bioconductor.org/packages/release/bioc/html/Cardinal.html) for image visualization and statistical analysis. Compound identifications are assigned based on both accurate mass and

isotope pattern matches to HMDB (Human Metabolome Database) (<3 ppm). Mean image intensities from corresponding radiated regions were compared using Student t-tests (2-tailed).

Hematoxylin and Eosin Staining of brain tissue sections

Ten micron cryosections from tumor-bearing brains were stained with Hematoxylin and Eosin (H&E) according to the manufacturer's instruction (Abcam; cat# ab245880). Briefly, sections were fixed with 4% PFA in PBS for 10 minutes then washed twice in PBS. Slides were incubated with Hematoxylin, Mayer's (Lillie's Modification) for 2 minutes at room temperature, then rinsed twice in distilled water to remove the excess of stain. Next, slides were incubated with Bluing Reagent for 10-15 seconds, rinsed twice with distilled water and dip in absolute alcohol. After blotting the excess off the slide, Eosin Y Solution (Modified Alcoholic) was applied to cover the brain sections and incubated for 2 minutes. Slides were then rinsed with absolute alcohol, dehydrated with three changes of absolute alcohol, cleared in xylene and mounted for analysis.

Evaluation of intracellular neutral lipids

To determine the content of neutral lipids in irradiated glioblastoma cells, $1x10^6$ GL261 and CT2A were plated in a 10-cm tissue culture dish on day 0. Twenty four hours after incubation, cells received a radiation dose escalation from 0Gy to 10Gy using the SARRP (open field, 2.82 Gy/min). Immediately after radiation, medium was replaced from each dish, including the control. Twenty four hours, 2 days, 3 days, 6 days or 7 days after irradiation, cells were collected and stained for neutral lipids by BODIPY™ 493/503 (4,4-Difluoro-1,3,5,7,8-Pentamethyl-4-Bora-3a, 4a-Diaza-s-Indacene; ThermoFisher Scientific; cat# D3922) or HCS LipidTOX™ Red Neutral Lipid Stain (ThermoFisher Scientific; cat# H34476) according to the manufacturer's intructions. Briefly, cells were trypsinized, washed with PBS, and incubated with 10μM of BODIPY or 1: 200 LipidTOX staining solution in PBS in the dark for 15 min at 37°C. After incubation, cells were

washed with PBS. Cells were then centrifuged for 5 min at 340 x g and resuspened with 200μL of 4% PFA in PBS (Santa Cruz Biotech, cat# sc-281692). All samples were acquired with a MACSQuant Analyzer 10 flow cytometer and analyzed with FloJo software version 10.4.0 (Tree Star). Results are displayed as mean fluorescence intensity with n=3 per group. Experiments were done at least in two biological experiments.

For LipidTOX staining for microscopy, $1.3x10^4$ GL261 or $1.8x10^4$CT2A cells were plated in 24-well plates with 12mm glass round coverslips on day 0. Twenty four hours after incubation, cells were exposed to 0 Gy or 10 Gy using the SARRP (open field, 2.82 Gy/min). Immediately after irradiation, medium was replaced in each dish, including the control. Twenty four hours after irradiation, cells were washed with PBS, and incubated with 1:200 LipidTOX staining solution in PBS in the dark for 15 min at 37°C. After incubation, cells were washed with PBS and then fixed with 4% PFA in PBS for 30 min at room temperature. Coverslips were mounted onto glass slides using a mounting medium containing DAPI (Vector Laboratories, cat# H-1800). Images were obtained using a Zeiss Axioplan Upright Wide Field Microscope at the Weill Cornell Medicine Optical Microscopy Core Facility.

Transmission Electronic microscopy

GBM cells were incubated with 4μg/mL of doxycycline 10 days prior to treatment to induce the knowckdown of *Fasn*. Next GL261 or CT2A derivatives were irradiated with a radiation dose of 0Gy or 10Gy. Twenty four hours after irradiation, cells were washed and fixed for 30 minutes in 2.5% glutaraldehyde, 4% paraformaldehyde and 0.002% of picric acid. Next, cells were washed with PBS and post-fixed with osmium (2% osminumtetroxide, 3 K-ferricyanide, 1:1 aqu) for 30-60 minutes at room temperature. The cells were then washed and stained en-bloc with 1.5% uranul acetate (aqu) for 30 minutes followed by dehydration in graded ethanol series 50%, 70%, 85%. 95%, 3x100% (5-10 min at each step). The cells were finally embedded in Epon-analog resin

comprised of 9.7 g of LX112 (Ladd Research Industries), 3.2g of DDSA (Electron microscopy sciences), 5.9 g of NMA (Electron microscopy sciences) and 34mL/mL of BDMA (Elextron microscopy sciences). Sections (1μm) were produced on a EM UC6 ultramicrotome and stained with 2% uranyl acetate and Reynold's lead citrate. Transmission electronic microscopy (TEM) was performed on JEM-1400 transmission electron microscope at 80 kV. These experiments were perfomed at the Weill Cornell Medicine Microscopy Core Facility.

Quantification of HMGB1

GBM cells were incubated with 4μg/mL of doxycycline 10 days prior to treatment to induce the knockdown of *Fasn*. Next, $0.5x10^5$ cells of GL261 or CT2A derivatives (i.e. GL261shNS and GL261shFASN) were plated in a 10-cm dish on day 0. Twenty four hours after incubation, cells received a radiation dose of 0 Gy or 10 Gy (n=3 per condition; SARRP; open field, 2.82 Gy/min). Immediately after irradiation, medium containing doxycycline was replaced in each dish, including the control. Twenty four hours after completion of tumor cells irradiation, supernatants were collected and live cells were counted using Trypan Blue. Next, HMGB1 was measured in cell-free supernantants using an enzyme-linked immunosorbent assay (Tecan HMGB1 ELISA, cat# ST51011, Fisher Scientific) following the manufacturer's instructions. Results were normalized by the number of live cells.

Western Blot

Proteins from GL261 and CT2A were extracted in RIPA buffer (Sigma, cat# R0278-50mL) containing a protease inhibitor cocktail (Sigma, cat # 11836153001) and a phosphatase inhibitors cocktail (ThermoFisher Scientific, cat # 78420). Protein concentrations were determine with BCA method (ThermoFisher Scientific, cat # 23227). A total of 30-50μg of protein of each sample was loaded in on a 8-10% SDS-PAGE and run at 100V constant voltage. Transfer of protein on

activated PVDF membrane (EMD-Millipore, cat#IPVH07850) were performed overnight at 4°C at 50mA. PVDF membraned were probed with primary antibodies (m-h-anti-BIP 1:1000, cat #3177T; m-h-anti-CHOP 1:1000, m-h-anti-fatty acid synthase 1:100, cat#3180T; m-h-anti-vinculin 1:1000, cat#13901S; Cell Signaling Technology) at 4°C overnight. Blots were incubated with ECL anti-rabbit IgG secondary antibody (Sigma, cat# GENA934-1 mL; 1:5000) at room temperature for 1 hour. Chemiluminescence was used to visualize protein bands (Perkin Elmer, cat# NEL103001EA). Pictures were acquired using the Azure c600 imager (Azure Biosystems). Precision Plus Protein™ Western C™ Blotting standards and Precision Protein™ Streptactin-HRP conjugate were used to estimate molecular weigh (BioRad, cat# 1610380 and cat#1610376). Relative quantification was performed using ImageJ software(version 1.53p (20)) to determine the protein expression ratios for each sample.

Immunostaining of GBM cells

$1.3x10^3$ GL261 and $1.8x10^3$ CT2A cells were plated in 24-well plates with 12mm glass round coverslips on day 0. Twenty four hours after incubation, cells were exposed to 0 Gy, 6 Gy and 10 Gy using the SARRP (open field, 2.82 Gy/min). Immediately after irradiation, medium was replaced in each dish, including the control. Twenty four hours after irradiation, cells were fixed with 4% PFA in PBS (Santa Cruz Biotech, cat# sc-281692). Cells were permeabilized and blocked simultaneously with 1% BSA (Gemini Bio-Products, cat# 700-100P), 10% normal goat serum (Cell Signaling Technology, cat# 5425S), 0.3M glycine (Bio-Rad, cat# 161-0717), 0.1%Triton X-100 (Fisher, cat# PB151) in PBS for for 1 hour at room temperature. Cells were incubated with a primary anti-FASN antibody diluted in 1%BSA PBS-0.05%Tween 20 (Abcam, cat# ab22759; 1:200) or Normal Rabbit IgG for the isotype control (Cell Signaling, cat# 2729; 1:200) overnight at 4°C. After three washes in PBS-0.05%Tween 20, samples were incubated with a secondary antibody diluted in 1%BSA PBS-0.05%Tween 20 (goat anti-mouse IgG H&L – Alexa fluor 488

preabsorbed, Abcam, cat# ab150081; 1:500) for 1 hour at room temperature. After 2 washes in PBS-0.05%Tween 20 then 2 washes in PBS, mounting medium containing DAPI was used (Vector Laboratories, cat# H-1800) to counterstain nuclei. Images were obtained using a Zeiss Axioplan Upright Wide Field Microscope at the Weill Cornell Medicine Optical Microscopy Core Facility .

Semi-automated quantification of FASN expression was performed by using Fiji software (v 1.53n; (21)) on at least 10 images for each condition . Integrated density was measured for all the cells of each images using a threshold to exclude the background. Then, the sum of the integrated density of an image was divided by the number of nucleus counted in that image in order to obtain the mean integrated density of cell per image.

Flow Cytometry Analysis of Apoptotic and Necrotic Cells

To determine the induction of apoptosis and necrosis in irradiated GBM cells, $1x10^6$ GL261 and CT2A derivatives (i.e. GBMsgControl and GBMsgFASN) were plated in a 10 cm tissue culture dish on day 0. Twenty four hours after incubation, cells received a radiation dose of 0 Gy or 10 Gy (n=3 per condition; SARRP; open field, 2.82 Gy/min). Immediately after irradiation, culture medium was replaced in each dish, including the control. Twenty four hours after irradiation cells were trypsinized and stained using the FITC Annexin V Apoptosis Detection Kit with PI (Biolegend, CA) following the manufacturer's instructions. All samples were acquired with a MACSQuant Analyzer 10 flow cytometer and analyzed with FloJo software version 10.4.0 (Tree Star). Cell populations were separated as follows: Apoptotic cells: Annexin V+/PI-, Necrotic cells: Annexin V+/PI+ and expressed as % of total single cells.

Processing of human glioblastoma microarray data

Glioblastoma expression data from The Cancer Genome Atlas (TCGA) was downloaded using GlioVis (version 0.2, http://gliovis.bioinfo.cnio.es/). The TCGA_GBM microarray dataset we used

was generated via the Affymetrix HG-U133A platform (22). According to the GlioVis pipeline, the raw .CEL files (when available) were downloaded from the respective sources and the analyses were completed in R using the Bioconductor suite. The Affy(23) package was used for robust multi-array average normalization followed by quantile normalization. For genes with several probe sets, the median of all probes had been chosen. In case the raw data was not available, the available pre-processed expression matrices were used.

In order to focus on the differences between primary and recurrent glioblastoma tumors, non-tumors, secondary tumors, and samples without annotated histology and recurrence information were excluded from downstream analyses. After filtering, we analyzed 513 tumors, 497 primary and 16 recurrent.

Differential gene expression and gene set enrichment analyses of recurrent and primary human glioblastoma tumors

Differential gene expression analysis comparing recurrent to primary human GBM tumors was conducted using LIMMA(24). lmFit() and eBayes() with default parameters were used for linear modeling and empirical Bayes moderation of standard errors, respectively. topTable() was then used to extract the differential expression outcomes for all genes in the dataset, including log2 fold changes and adjusted p-values after Benjamini-Hochberg correction. As our paper highlights the role of lipid metabolism, we then selectively isolated the differential expression of genes listed in REACTOME's metabolism of lipids gene signature (https://reactome.org/content/detail/R-HSA-556833) and visualized using a volcano plot(25).

For geneset enrichment analysis (GSEA version 4.2.3, Broad institute)(26,27), we focused more specifically on fatty acid biosynthesis using a canonical Wikipathways signature (https://www.wikipathways.org/index.php/Pathway:WP357). All expression data from both recurrent and primary GBM tumors were used as input and GSEA was run with default parameters with no_collapse to gene symbols and gene_set as the permutation type.

Statistics

All statistical analyses were performed using GraphPad Prism 9 and are considered significant when $p<0.05$. The identity of the statistical test performed, p values and n values are stated in the figure legends. One-way Analysis of Variance (ANOVA) followed by Tukey's post hoc multiple comparisons was applied for statistical analysis of neutral lipids accumulation, free fatty acid profiles, HMGB1 quantification, TEM analysis of mitochondria, targeted metabolic profiles, FASN expression by immunocytochemistry, flow cytometry analysis of apoptotic and necrotic cells and metabolic fuel flux. Unpaired student's t test was applied for statistical analysis of Seahorse MitoStress Assay and MALDI-IMS.

RESULTS

RT enhances bioenergetic capacity and fuels flexibility of irradiated GBM cells

Mitochondria can adapt in response to cues from the TME to sustain cellular energy in the form of ATP produced by oxidative phosphorylation (OXPHOS). The bioenergetic parameter of mitochondrial fitness is the spare respiratory capacity (SRC), which is the extra mitochondrial capacity available in a cell to produce energy under genotoxic stressors such as RT. To explore whether RT impacts the bioenergetic demand of GBM, we first used Seahorse XF analyzer Mito Stress assays to evaluate mitochondrial function in two murine GBM cell lines (GL261 and CT2A). Irradiation of GBM cells significantly increased basal and maximal oxygen consumption rate (OCR) and extra cellular acidification rates (ECAR) indicative of enhanced mitochondrial respiration and glycolysis of GBM cells post 10 Gy RT (Fig. 1A and 1B). As anticipated, these observations resulted in a significant increase of ATP and SCR in irradiated GBM cells.

To identify which oxidative pathway was responsible for the enhanced basal energetic demands in irradiated GBM cells, we investigated the relative contributions of glucose, glutamine and long-chain fatty acid oxidation (FAO) to basal respiration by Seahorse XF Mito Fuel Flex assays. As expected, both GL261 and CT2A mainly rely on glucose consumption as a mitochondrial fuel (Fig. 1C and 1D). Surprinsingly, RT did significantly enhance the contribution of glucose in GL261 but not in CT2A. Interestingly, the ability to consume glutamine and fatty acids in basal respiration was increased in both cell line post RT 24hrs after RT (Fig. 1C and 1D). Of note, in both cell lines, fatty acid oxidation was the most altered with up to a 3-fold increase post RT (Fig. 1C and 1D). These data demonstrate that irradiation of GBM cells is associated with a greater bioenergetic capacity and fuel flexibility.

RT increases mitochondrial activity to use alternative pathways as energy sources

To further investigate RT-induced metabolic changes in GBM cells, targeted detection of metabolites belonging to glycolysis, tricarboxylic acid (TCA) intermediates and amino acids were performed in GL261 cells 24hrs post 0, 6 and 10 Gy irradiation. Unsupervised principal component analysis (PCA) revealed that replicates from the same group were closely related and can be distinguished from other radiation groups (Fig. 1E), with principal component 1 resolving 80.7% of the variability. Based on the degree of similarity of metabolite abundance profiles, hierarchical clustering analysis was performed to show the global view of all metabolites detected in GL261 across radiation groups using MetaboAnalyst 5.0 software. The heatmap revealed that 64 metabolites were differentially expressed with a dose-dependent increase in the intensity of most metabolites (Fig. 1G and Supplementary Table 1). Metabolite set enrichment analysis was then performed to identify the most enriched metabolic pathways in GL261 cells. As expected, pathways that reflect DNA damage (28-30), namely the aminoacyl-tRNA biosynthesis, pentose phosphate and nicotinamide, were showed high levels of enrichment (Fig. 1F). Importantly, consistent with our previous data (Fig. 1B), the glutamine metabolism was significantly enriched in response to RT (Fig. 1F).

Altogether, these results show that RT increases mitochondrial activity and the ability to use alternative pathways as energy sources such as glutamine and fatty acid oxidation.

RT perturbs the metabolism of GBM to promote the generation of unsaturated fatty acids

Because glutamine is a well-known carbon source for *de novo* lipogenesis(31) and RT increases the contribution of fatty acids (FAs) to cope with energy demand (Fig. 1C and 1D), we determined the free fatty acid profiles 24hrs post RT in irradiated GBM cells (Fig. 2 and Supplementary Table 2). Out of the 40 fatty acids we probed, all of them were expressed in GBM cells with a baseline

expression more pronounced in GL261 as compared to CT2A (Supplementary Fig. 1). Interestingly, RT significantly increased the overall expression of all FAs. However, unsaturated fatty acids (UFAs) were the most altered in response to genotoxic stress from RT. Specifically, our data shows that RT significantly promotes UFAs such as oleic acid (C18:1), linoleic acid (C18:2), arachidonic acid (AA; C20:4), eicosapentaenoic acid (EPA; C20:5) and docohexaenoic acid (DHA; C22:6) (Fig. 2B and 2D).

The magnitude of metabolic changes may be linked to variables pertaining to the TME including, but not limited to, hypoxia and the availability of nutrients. In that context, to confirm that RT was altering GBM metabolism towards the generation of UFAs *in vivo*, we performed mass spectrometry imaging of brain sections bearing CT2A tumors. To that end, C57BL/6N mice bearing intracranial GBM received tumor targeted irradiation given in a single fraction of 10 Gy on day 10. Brains were harvested on day 15 for spatial metabolomic analysis (Fig. 3A). Unsupervised PCA showed that replicates from the same group were closely clustered and that irradiated CT2A tumors can be distinguished from control (PC1 90.2%, Fig. 3B). The heat map indicated that 103 metabolites were significantly differentially altered in irradiated CT2A tumors (Fig. 3C and Supplementary Table 3) and confirmed the increase of metabolites linked to glycolysis, pentose phosphate and TCA cycle (e.g. aconitic acid and succinic acid). Additionally, supporting our *in vitro* data, results indicate that RT enhanced glutamine and lipid metabolism with overexpression of metabolites belonging to glutamine/glutamate (e.g. glutamine and glutamic acid) and free fatty acid pathways (Fig. 3C and 3D). Specifically, further validating our *in vitro* data, several UFAs were significantly upregulated in irradiated CT2A tumors, including DHA, AA and lysophosphatidic acid (LPA; C22:6) (Fig. 3D). Of note, even though some glycerolipids were decreased in response to RT, the majority were over-represented in CT2A tumors (Fig. 3C and 3D).

Overall, these results show that RT promotes a cellular pool of UFAs that can later serve as building blocks for glycerolipids such as phosphatidic acid (PA), phosphatidylserines (PS), phosphoethanolamines (PE), sphingomyelin and eicosanoids.

Accumulation of FAs promotes lipid droplets in irradiated GBM cells

Excess of FAs induces lipotoxicity that is associated with endoplasmic reticulum (ER) stress, mitochondrial dysfunction and cell death (32). To prevent this from occurring, cancer cells may generate lipid droplets (LD), a lipid-rich organelle. LDs store neutral lipids, mostly triacylglycerol (TAG) and cholesteryl esters, and balance FA uptake, storage and use according to the energy demands. It has been demonstrated that LDs act as transient buffers that reduce FA lipotoxicity (33). In that context, we asked whether RT-induced FAs result in the formation of LDs to counteract lipotoxicity and support GBM survival in response to RT. To test this hypothesis, we subjected two murine (GL261 and CT2A) and one human (U118) GBM cell lines to a radiation dose escalation and determined the accumulation of neutral lipids by BODIPY and LipidTOX stainings. We found that irradiation of GBM cells results in a significant increase of lipids in a dose-dependent fashion (Fig. 4A and 4B). Visualization of LDs in irradiated murine GBM cells confirmed the enhanced formation of LDs 24hrs post RT (Fig. 4C). Next, to evaluate whether this effect was maintained over time, we assessed the accumulation of neutral lipids up to 7 days after RT. Our data demonstrated a sustained increase of lipids in irradiated GBM cells, an effect that is magnified over time in all the cell lines we tested (Fig. 4D).

Overall, these findings show that RT induces neutral lipid accumulation and storage, an effect that persists for at least 7 days *in vitro*.

Radiation-induced FASN is responsible for the accumulation of lipids in irradiated GBM

Because fatty acid synthase (FASN) is responsible for the *de novo* production of most (if not all) unsaturated lipids (Fig. 5A) (34), we asked whether FASN modulates the synthesis of lipids post-RT in our system. We first irradiated GL261 and CT2A and determined the protein expression of FASN by immunofluorescence. Our data showed an upregulation of FASN in GBM cells 24hrs post RT (Fig. 5B). To ask whether FASN was responsible for the accumulation of lipids in irradiated GBM cells, we generated CRISPR/Cas9 engineered sgControl (control) or sgFasn (Fasn inactivation) CT2A and GL261 cells. FASN deficiency was validated by western blot (Supplementary Fig. 2A).

In line with our previous data, irradiated but not control GBM cells accumulated neutral lipids in both GL261 and CT2A. Interestingly, confirming the role of FASN in the RT-induced generation of lipids, lipid accumulation was significantly reduced in FASN-deficient GBM cells. Of note, the decrease of neutral lipid accumulation was not complete in GBM-sgFasn cells, suggesting that another pathway might promote lipid accumulation in irradiated GBM (Fig. 5C).

Lipid accumulation limits endoplasmic reticulum stress and apoptosis of irradiated GBM

Reports indicate that excessive synthesis of lipids is an adaptive mechanism of ER to cope with cell stress and avoid apoptosis (35-37). Our results indicate that RT is eliciting a lipogenic phenotype in GBM (Figs. 2-4). Thus we asked whether FASN-mediated lipid synthesis is a resistance mechanism that resolves ER stress in irradiated GBM cells. To test this hypothesis, we used CRISPR/Cas9 and shRNA-mediated FASN knockdown (KD) cells. GL261 and CT2A derivatives with selective KD of FASN using a doxycycline (DOX) inducible construct (Supplementary Fig. 2B). The shRNA was introduced into a pTRIPZ inducible lentiviral shRNA

vector containing the tetracycline response element (TRE) promoter, which leads to shRNA expression in the presence of DOX.

Having confirmed the KD of FASN in GBM cells (Supplementary Fig. 2C), we investigated the role of FASN-mediated lipid synthesis and ER stress in irradiated GBM cells. Hallmarks of ER stress are, but not limited to, loss of mitochondrial integrity and the activation of the unfolded protein response (UPR) pathway (38). We first analyzed mitochondria by transmission electronic microscopy (TEM) in GL261 and CT2A derivatives 24hrs post RT. Our data revealed a loss of mitochondrial shape and a decrease of their crypts in FASN-deficient GBM cells, indicative of a mitochondrial dysfunction. Interestingly, irradiation did not enhance this effect, thus suggesting that the absence of FASN alone can perturb the energy supply of GBM cells (Fig. 5D).

The UPR pathway is triggered by the onset of ER stress to restore cell homeostasis (39). There are three primary branches of the UPR pathway and each is mediated by distinct ER proteins namely inositol-requiring enzyme 1 (IRE1), protein kinase R-like endoplasmic reticulum kinase (PERK) and activating transcription factor 6 (ATF6) (39). During ER stress, the ER chaperone BiP (immunoglobin binding protein) dissociates from these ER stress transducers leading to their activation. If ER protein homeostasis is not resolved, the prolonged activation of UPR may initiate apoptosis via the upregulation of the C/EBP Homologous Protein (CHOP). Therefore, to interrogate whether RT-induced FASN is controlling ER stress, we determined the expression of BiP and CHOP 24 hrs post RT in GBM-sgFasn cells. Tunicamycin (2 μg/mL) was added to GBM cells to induce ER stress as a positive control. A slight baseline protein expression of BiP and CHOP was observed in untreated or irradiated GBM cells. However, the absence of FASN markedly increased BiP and CHOP in untreated GBM cells, an effect that was amplified in irradiated GBM (Fig. 5E).

Although evidence indicates that FASN can resolve ER stress of irradiated GBM cells (Figs. 5D-5E), it is still unclear whether it protects them from cell death. To address this question, we first measured the extracellular release of High mobility group box protein 1 (HMGB1), a damage-associated molecular pattern (DAMP) that is emitted by dying cells, 24 hours post RT. As expected, RT increases the release of HMGB1 in both GBM cells. FASN KD promoted extracellular accumulation of HMGB1 in GL261 but not in CT2A cells. Interestingly, HMGB1 release was enhanced in irradiated FASN-deficient GL261 and CT2A cells (Fig. 5F), suggesting that cytocidal properties of RT might be improved when FASN is impaired. To test this hypothesis, we determined apoptosis and necrosis 24hrs after irradiation. As expected, we found that apoptosis and necrosis were greater in GBM-sgFasn cells as compared to sg-Control cells. Interestingly, RT significantly increased apoptosis but did not further promote necrosis in both FASN deficient GBM cells (Fig. 5G).

Overall, these results indicate that FASN-mediated lipid accumulation prevents ER stress and evades apoptosis to cope with genotoxic insult and promote survival of irradiated GBM.

Fatty Acid biosynthesis gene signature is enriched in recurrent GBM patients

To test the translational value of our findings, we performed analysis on a publicly available human GBM dataset - TCGA HG-UG133A glioblastoma (GBM) dataset. As recurrent GBM patients were previously treated with standard RT and temozolomide (TMZ), we hypothesized that recurrent GBM patients would exhibit an increased lipid metabolism signature as a response to RT+TMZ treatment. To address this question, using the Metabolism of Lipids pathway from REACTOME (Supplementary Table 4), we compared primary GBM (n=497) to recurrent GBM (n=16) and found increased expression of genes envolved in fatty acid synthesis (SLC27A2 logFold Change (FC) = 0.712, p = 8.97E-6; ECHS1 FC = 0.529, p=3.38E-6; FASN FC = 0.307, p = 0.004), UFAs

synthesis (SCD FC = 0.507, p = 0.023; SCD5 FC = 0.888, p = 4.87E-6), glycerophospholipids and triglycerides synthesis for LD formation (AGPAT2 FC = 0.517, p = 0.0001), sphingolipid synthesis (ORMDL2 FC = 0.644, p = 0.0005), and eicosanoid synthesis (PTGES2 FC = 0.531, p = 4.08E-6; PTGES FC = 0.757, p = 1.02E-5; HPGD FC = 0.552, p = 0.007; AKR1C2 FC = 1.016, p = 0.048) (Fig. 6A, Supplementary Tables. 5 and 6). This is consistent with our data that indicate an increase of UFAs, polyunsaturated fatty acids as upstream of eicosanoid synthesis (namely AA, EPA and DHA) (Figs. 2-3) and an accumulation of neutral lipids and LD post RT (Fig. 4).

To further evaluate fatty acid biosynthesis we performed geneset enrichment analysis (GSEA) of the WikiPathways (WP) Fatty Acid Biosynthesis pathway (Supplementary Table. 4) comparing primary GBM to recurrent GBM, and found increased enrichment of this pathway in recurrent cases (Fig. 6B, enrichment score = 0.547, p-value = 0.019).

Overall, these data are consistent with our preclinical findings and supports the relevance of targeting lipid metabolism in human GBM to decrease resistance to RT and limit GBM recurrence.

DISCUSSION

RT is the standard-of-care for the management of GBM and is the only effective treatment for inoperable brain tumors. However, GBM relapses often arise within the irradiated margins (7), suggesting that the TME of GBM post RT generates resistance mechanisms that may support GBM recurrence. The mechanisms by which RT drives GBM regrowth remain elusive.

Here, we showed that RT provides metabolic plasticity for GBM to survive genotoxic insults and acquire adaptive resistance mechanisms. Specifically, we identified the biosynthesis of fatty acids as a dominant metabolic pathway that protects irradiated GBM cells from undergoing ER stress; thereby permitting the escape of RT-induced apoptosis. These results have important implications for the use of lipid metabolism targeting agents in patients, and suggests that combination of RT with such compounds might be required to develop treatments that are more effective and resistant to GBM recurrence.

Prior research conducted in pancreatic tumors demonstrated that mitochondrial activity and OXPHOS are activated in resistant tumors to survive anti-cancer modalities such as RT (40). Supporting this notion, our findings demonstrate that mitochondria activate OXPHOS to generate lipids and cope with the energy demand post RT. Specifically, the ability to use FAO for basal respiration was increased in both of our murine GBM cell models despite the fact that they displayed disctinct metabolic profiles at baseline. These results are in line with a previous study in which FAO was identified as a dominant metabolic program that provides GBM metabolic flexibility to adapt to the nutrient heterogeneity of its TME (41). We also found that irradiated GBM (both *in vitro* and *in vivo*) rewires its energy supply towards the synthesis of UFAs to presumably generate a cellular pool of fatty acids that can be utilized as building blocks for complex lipids involved in structure, fluidity and function of the cellular membrane. Similar findings have been reported in the field of radiation countermeasures where a specific lipidomic signature (mostly

belonging to polyunsaturated UFAs) was identified in serum of healthy mice exposed to a radiation dose of 8 Gy (42).

Importantly, our findings demonstrate that accumulation of UFAs in response to RT leads to the formation of LDs, which are major sites for prostaglandin E2 (PGE2) synthesis and have been ascribed roles in tumor cell proliferation, cancer stemness and immunosuppression (43-45). Our *in silico* analysis of recurrent GBM patients confirms the increase of prostaglandins with significant upregulation of prostaglandin E2 synthase (PTGES2) and prostaglandin E synthase (PTGES), thus underscoring that RT might promote the formation of UFAs to synthesize eicosanoids, and more specifically the prostanoid family of lipids in recurrent GBM patients.

Our study suggests that the biological implications of lipid metabolism reprogramming subsequent to tumor targeted irradiation are to protect GBM from apoptosis by resolving ER stress. Consequently, RT-induced lipid metabolism may drive resistance of GBM. With limitations pertaining to retrospective *in silico* studies, our findings support this concept with a significant enrichment of fatty acid biosynthesis in recurrent GBM patients. Additionally, while the clinical relevance of our findings need to be validated, our study suggests that combination of lipid metabolism inhibitors with ER stress inducers may represent a novel strategy to prolong survival of irradiated GBM patients.

PGE2 is known to play a role in regulating inflammation that drives cancer initiation and progression. Several studies have shown that PGE2 can activate growth factor signaling, resistance to apoptosis and enhance immune evasion (46). PGE2 is the major product of the cyclooxygenases (COXs). While COX-1 is constitutively at basal levels of many cells, COX-2 is induced in response to several stimuli to mediate pathological events that are associated with inflammatory processes (47). In fact, GBM highly expresses COX-2 which led to the development

of COX-2 inhibitors such as celecoxib. Celecoxib is a COX-2 inhibitor well-known to induce ER stress. However, in a randomized phase II clinical trial with newly diagnosed GBM patients, RT+TMZ combined with celecoxib failed to improve patients' overall survival (NCT00112502, (48)). Based on our data, it is plausible that celecoxib was unable to induce ER stress due to RT-induced FASN metabolism in these patients. Further, dual blockade of celecoxib with FASN inhibition promotes ER stress and subsequent cell death in mucinous colon cancer (49). As FASN inhibitors are actively tested in clinical trials for multiple tumors including GBM (NCT03808558, NCT02980029, NCT03179904, NCT03032484), this work supports the use of these compounds to enhance the efficacy of ER stress inducers as well as COX-2 inhibitors to potentially prolong the survival of GBM patients.

On another note, PGE2, has also been reported to promote an immunosuppressive phenotype of tumor-associated macrophages (TAMs) by initiating a signal transduction cascade to increase the programmed death-ligand 1 (PD-L1) transcriptional levels of TAMs (45). Our work shows that (i) arachidonic acid, a precursor for PEG2 synthesis, is overexpressed post RT and (ii) prostaglandin E2 synthase (PTGES2) is upregulated in recurrent GBM patients. Thus, it is conceivable that FASN upregulation in response to RT is a major obstacle to the efficacy of anti-programmed death-1 (PD-1) in GBM. Previous clinical trials targeting PD-1 alone led to only 8% of objective response rate in recurrent GBM (Checkmate 143) (50). As all patients from Checkmate 143 received prior RT and TMZ, it is possible that RT-induced FASN may have driven PGE2-mediated immunosuppression to limit anti-PD-1 efficacy in these patients. While further evidence are warranted, our work also support the combination of FASN inhibitors with PD-1 blockade to improve the outcome of GBM patients in the context of RT.

In conclusion, our results identify the role of lipids in providing metabolic plasticity of irradiated GBM, therefore allowing GBM cells to accommodate to genotoxic stress and develop resistance

mechanisms by at least icreasing UFAs to synthesize eicosanoids, and more specifically the prostanoid family. Overall these data underscore the role of UFAs in shaping the TME and cancer progression of irradiated GBM. Although the role of UFAs in RT-induced resistance of GBM remains to be confirmed, our data provide the rationale for testing UFA targeting agents in the clinic, and highlight a potential new actionable target to improve response in GBM patients post RT.

ACKNOWLEDGMENTS

We are acknowledging the Proteomics and Metabolomics Core Facility for their assistance in profiling free fatty acids in irradiated murine glioblastoma cells. We are grateful to the Electron Microscopy & Histology services of the Weill Cornell Medicine Microscopy & Image Analysis Core for their assistance in transmission electronic images.

FIGURE LEGENDS

Figure 1: **Radiation induces metabolic reprogramming in glioblastoma cells.** Murine glioblastoma cells GL261 and CT2A were analyzed 24hrs after irradiation (10Gy) by extracellular flux analysis. Fundamental mitochondrial function was determined by Seahorse MitoStress Assay for oxygen consumption rate (OCR) and extracellular acidification rate (ECAR) at baseline and in response to sequential injections of oligomycin (O), FCCP (F), and rotenone with antimycin (R/A) in GL261 (**A**) and CT2A (**B**). OCR was used to quantify ATP production and spare respiratory capacity (SRC). Substrate fuel capacity for the three major fuel pathways of glucose (GLC), glutamine (GLN) and fatty acid (FA) was determined by Seahorse Mito Fuel Flex Test in GL261 (**C**) and CT2A (**D**). Values represent mean ± SEM. ns, not significant; **p<0.01; ***p<0.001; ****p<0.0001, using unpaired Student's t test (**A** and **B**), or one-way ANOVA followed by Tukey post hoc comparisons (**C** and **D**). (**A – D**) Experiment was done in duplicate with n=6-12 per group. (**E – G**) GL261 cells were analyzed by targeted metabolic profiling 24hrs after irradiation with 6Gy or 10Gy. Metabolites commonly detected in two independent (n=3/group) experiments were combined for analysis. (**E**) PCA score plots. (**F**) Heatmap of differentially expressed metabolites in 6Gy and 10Gy. (**G**) Pathway enrichment analysis in common metabolites between two independent experiments. Experiment was done in duplicate with n=3 per group.

Figure 2: Unstaturated fatty acids are preferentially induced by irradiation of glioblastoma cells *in vitro*. GL261 and CT2A cells were subjected to 6Gy or 10Gy irradiation *in vitro* and 24hrs later cells were collected for free fatty acid profiling by mass spectrometry. Heatmap of differentially expressed fatty acids in averaged replicates (n=5/group) in CT2A (**A**) and GL261 (**C**) cells. Peak intensity of representative saturated, monounsaturated, and polyunsaturated fatty acids for CT2A (**B**) and GL261 (**D**) cells. Values represent mean ± SEM. Each dot represents one replicate. *p<0.05; **p<0.01; ***p<0.001; ****p<0.0001, using one-way ANOVA followed by Tukey post hoc comparisons (B and D). Experiment was done in duplicate with n=5 per group.

Figure 3: Radiation alters glioblastoma metabolism toward the generation of unsaturated fatty acids *in vivo*. (**A**) Experiment scheme and timeline. Briefly, 50.000 CT2A cells were injected i.c. into C57BL/6N mice on day 0 (n=3/group). On day 10, radiation was selectively given to i.c. tumors in a single dose of 10 Gy. On day 15, tumor-bearing brains were collected for MALDI imaging. (**B**) PCA score plots. (**C**) Heatmap of differentially expressed metabolites in 10Gy irradiated tumors. (**D**) H&E of brain sections from animals in (A). Scale 5mm. Peak intensity and representative images of metabolites. Values represent mean ± SEM. Each dot represents one animal. *p<0.05; **p<0.01; ***p<0.001, using unpaired Student's t test (D).

Figure 4: Radiation induces accumulation of lipid droplets in glioblastoma cells. (**A**) Murine glioblastoma GL261 and CT2A cells and human glioblastoma U118 cells were subjected to different radiation doses from 2Gy to 10Gy *in vitro* and 24hrs later, neutral lipids accumulation was determined by BODIPY (495/503) staining and flow cytometry. (**B**) Flow cytometry analysis of LipidTOX staining in GL261 and CT2A 24hrs after 10Gy irradiation. (**C**) Representative images and quantification of LipidTOX fluorescence staining for 10Gy irradiated GL261 and CT2A cells. Scale 20µm. Lipid droplets are pointed with white arrows. (**D**) Glioblastoma cells were plated on day 0 and subjected to 10Gy irradiation at different time points (from 1 to 7 days before collection) to synchronize the collection and BODIPY staining on the same day. Values represent mean ± SEM. Each dot represents one replicate. *p<0.05; **p<0.01; ***p<0.001; ****p<0.0001, using one-way ANOVA followed by Tukey post hoc comparisons (A, B and D) or unpaired Student's t test (C). Experiment was done in duplicate with n=3 per group.

Figure 5: Radiation-induced FASN is responsible for the accumulation of lipids and prevents ER stress and apoptosis in irradiated GBM. (**A**) Overview of the main pathways responsible for the cellular fatty acid pool: de novo fatty acid synthesis and uptake. Highlighted in red are the components described to be modulated by radiation (Figures 1-5). (**B**) Representative

images and quantification of FASN immunofluorescence staining 24hrs after 6Gy and 10Gy irradiation in GL261 and CT2A cells. Scale 50μm. (**C**) Flow cytometry analysis of BODIPY 495/503 staining in CRISPR/Cas9 sgControl or sgFasn GL261 and CT2A cells 24hrs after 10Gy irradiation. (**D**) Representative transmission electron microscopy images and quantification of mitochondria without cristae in 10Gy irradiated shNon-silencing (shNS) or shFASN GL261 and CT2A cells. Scale 1 μm. (**E**) Western blot results showing expression of BIP and CHOP, in CRISPR/Cas9 sgControl or sgFasn CT2A cells 24hrs after 10Gy irradiation or sgControl cells treated for 24hrs with tunicamycin 2μg/ml. VINCULIN expression levels were used as a loading control. (**F**) HMGB1 secretion was determined by ELISA 24hrs after 10Gy irradiation of shNon-silencing (shNS) or shFASN GL261 and CT2A cells. Results are expressed in pg/mL ± SEM for 100,000 live cells. (**G**) Flow cytometry analysis of AnnexinV/PI staining in CRISPR/Cas9 sgControl or sgFasn GL261 and CT2A cells 24hrs after 10Gy irradiation. Values represent mean ± SEM. Each dot represents one replicate. ns, not significant; *p<0.05; **p<0.01; ***p<0.001; ****p<0.0001, using one-way ANOVA followed by Tukey post hoc comparisons (B-G). Experiment was done in duplicate with n=3 per group.

Figure 6: Fatty acid biosynthesis is enriched in recurrent glioblastoma tumors

A. Volcano plot shows differential expression of lipid metabolism related genes in recurrent (red) and primary (blue) GBM. Vertical grey lines delineate a log2 fold change (FC) of > 0.5 or < -0.5. Horizontal grey line represents an adjusted p-value of < 0.05 after Benjamini-Hochberg correction. **B.** Recurrent tumors demonstrate an enrichment in fatty acid biosynthesis (enrichment score = 0.547, nominal p-value = 0.019).

Supplementary Figure 1: Comparison of fatty acids baseline expression in glioblastoma cells. Differentially expressed fatty acids determined by free fatty acid profiling by mass

spectrometry in GL261 vs CT2A cells. One-way ANOVA followed by Tukey post hoc comparisons; *p<0.05; **p<0.01; ***p<0.001; ****p<0.0001. Experiment was done in duplicate with n=5 per group.

Supplementary Figure 2: Characterization of genetically modified glioblastoma cells. (**A**) Western blot analysis of FASN protein expression in GL261 and CT2A CRISPR/Cas9 sgControl or sgFasn clones, obtained with 2 different anti-Fasn guide RNAs. (**B**) Modified pTRIPZ lentiviral vector with tetracycline-inducible shRNA directed against the mouse *Fasn* gene (shFASN) or its non-silencing control (shNS). Fasn knockdown in GL261 and CT2A cells was confirmed by western blot 10 days after doxycycline induction (**C**).

Supplementary Table 1: Peak intensities of polar metabolites in irradiated GL261.

Supplementary Table 2: Peak intensities of free fatty acids in irradiated GL261 and CT2A.

Supplementary Table 3: Mean image intensities from corresponding tumor regions of Metabolites in CT2A and GL261.

Supplementary Table 4: Genesets Used for retrospective analysis of the TCGA GBM datasets

Supplementary Table 5: Differential gene expression of all genes in Recurrent versus Primary GBM patients.

Supplementary Table 6: Differential gene expression of metabolism of lipids pathway in Recurrent versus Primary GBM patients.

REFERENCES

1. Grech N, Dalli T, Mizzi S, Meilak L, Calleja N, Zrinzo A. Rising Incidence of Glioblastoma Multiforme in a Well-Defined Population. Cureus **2020**;12:e8195
2. Philips A, Henshaw DL, Lamburn G, O'Carroll MJ. Brain Tumours: Rise in Glioblastoma Multiforme Incidence in England 1995-2015 Suggests an Adverse Environmental or Lifestyle Factor. J Environ Public Health **2018**;2018:7910754
3. Stupp R, Mason WP, van den Bent MJ, Weller M, Fisher B, Taphoorn MJ*, et al.* Radiotherapy plus concomitant and adjuvant temozolomide for glioblastoma. N Engl J Med **2005**;352:987-96
4. Sulman EP, Ismaila N, Armstrong TS, Tsien C, Batchelor TT, Cloughesy T*, et al.* Radiation Therapy for Glioblastoma: American Society of Clinical Oncology Clinical Practice Guideline Endorsement of the American Society for Radiation Oncology Guideline. J Clin Oncol **2017**;35:361-9
5. Beauchesne P, Bernier V, Carnin C, Taillandier L, Djabri M, Martin L*, et al.* Prolonged survival for patients with newly diagnosed, inoperable glioblastoma with 3-times daily ultrafractionated radiation therapy. Neuro Oncol **2010**;12:595-602
6. Cabrera AR, Kirkpatrick JP, Fiveash JB, Shih HA, Koay EJ, Lutz S*, et al.* Radiation therapy for glioblastoma: Executive summary of an American Society for Radiation Oncology Evidence-Based Clinical Practice Guideline. Pract Radiat Oncol **2016**;6:217-25
7. Ogura K, Mizowaki T, Arakawa Y, Ogura M, Sakanaka K, Miyamoto S*, et al.* Initial and cumulative recurrence patterns of glioblastoma after temozolomide-based chemoradiotherapy and salvage treatment: a retrospective cohort study in a single institution. Radiat Oncol **2013**;8:97
8. Faubert B, Solmonson A, DeBerardinis RJ. Metabolic reprogramming and cancer progression. Science **2020**;368

9. Venneti S, Thompson CB. Metabolic Reprogramming in Brain Tumors. Annu Rev Pathol **2017**;12:515-45

10. Prabhu A, Kesarwani P, Kant S, Graham SF, Chinnaiyan P. Histologically defined intratumoral sequencing uncovers evolutionary cues into conserved molecular events driving gliomagenesis. Neuro Oncol **2017**;19:1599-606

11. Taib B, Aboussalah AM, Moniruzzaman M, Chen S, Haughey NJ, Kim SF*, et al.* Lipid accumulation and oxidation in glioblastoma multiforme. Sci Rep **2019**;9:19593

12. Tanaka K, Sasayama T, Irino Y, Takata K, Nagashima H, Satoh N*, et al.* Compensatory glutamine metabolism promotes glioblastoma resistance to mTOR inhibitor treatment. J Clin Invest **2015**;125:1591-602

13. Azzam EI, Jay-Gerin JP, Pain D. Ionizing radiation-induced metabolic oxidative stress and prolonged cell injury. Cancer Lett **2012**;327:48-60

14. Gupta K, Vuckovic I, Zhang S, Xiong Y, Carlson BL, Jacobs J*, et al.* Radiation Induced Metabolic Alterations Associate With Tumor Aggressiveness and Poor Outcome in Glioblastoma. Front Oncol **2020**;10:535

15. Newcomb EW, Lukyanov Y, Kawashima N, Alonso-Basanta M, Wang SC, Liu M*, et al.* Radiotherapy enhances antitumor effect of anti-CD137 therapy in a mouse Glioma model. Radiat Res **2010**;173:426-32

16. Panagioti E, Kurokawa C, Viker K, Ammayappan A, Anderson SK, Sotiriou S*, et al.* Immunostimulatory bacterial antigen-armed oncolytic measles virotherapy significantly increases the potency of anti-PD1 checkpoint therapy. J Clin Invest **2021**;131

17. Chen WW, Freinkman E, Wang T, Birsoy K, Sabatini DM. Absolute Quantification of Matrix Metabolites Reveals the Dynamics of Mitochondrial Metabolism. Cell **2016**;166:1324-37 e11

18. Pang Z, Chong J, Zhou G, de Lima Morais DA, Chang L, Barrette M*, et al.* MetaboAnalyst 5.0: narrowing the gap between raw spectra and functional insights. Nucleic Acids Res **2021**;49:W388-W96

19. Zeng J, See AP, Phallen J, Jackson CM, Belcaid Z, Ruzevick J*, et al.* Anti-PD-1 blockade and stereotactic radiation produce long-term survival in mice with intracranial gliomas. Int J Radiat Oncol Biol Phys **2013**;86:343-9

20. Schneider CA, Rasband WS, Eliceiri KW. NIH Image to ImageJ: 25 years of image analysis. Nat Methods **2012**;9:671-5

21. Schindelin J, Arganda-Carreras I, Frise E, Kaynig V, Longair M, Pietzsch T*, et al.* Fiji: an open-source platform for biological-image analysis. Nat Methods **2012**;9:676-82

22. Cancer Genome Atlas Research N. Comprehensive genomic characterization defines human glioblastoma genes and core pathways. Nature **2008**;455:1061-8

23. Gautier L, Cope L, Bolstad BM, Irizarry RA. affy--analysis of Affymetrix GeneChip data at the probe level. Bioinformatics **2004**;20:307-15

24. Ritchie ME, Phipson B, Wu D, Hu Y, Law CW, Shi W*, et al.* limma powers differential expression analyses for RNA-sequencing and microarray studies. Nucleic Acids Res **2015**;43:e47

25. Gillespie M, Jassal B, Stephan R, Milacic M, Rothfels K, Senff-Ribeiro A*, et al.* The reactome pathway knowledgebase 2022. Nucleic Acids Res **2022**;50:D687-D92

26. Mootha VK, Lindgren CM, Eriksson KF, Subramanian A, Sihag S, Lehar J*, et al.* PGC-1alpha-responsive genes involved in oxidative phosphorylation are coordinately downregulated in human diabetes. Nat Genet **2003**;34:267-73

27. Subramanian A, Tamayo P, Mootha VK, Mukherjee S, Ebert BL, Gillette MA*, et al.* Gene set enrichment analysis: a knowledge-based approach for interpreting genome-wide expression profiles. Proc Natl Acad Sci U S A **2005**;102:15545-50

28. Sobanski T, Rose M, Suraweera A, O'Byrne K, Richard DJ, Bolderson E. Cell Metabolism and DNA Repair Pathways: Implications for Cancer Therapy. Front Cell Dev Biol **2021**;9:633305

29. Ying W, Alano CC, Garnier P, Swanson RA. NAD+ as a metabolic link between DNA damage and cell death. J Neurosci Res **2005**;79:216-23

30. Song Y, Shi Y, Carland TM, Lian S, Sasaki T, Schork NJ*, et al.* p53-Dependent DNA damage response sensitive to editing-defective tRNA synthetase in zebrafish. Proc Natl Acad Sci U S A **2016**;113:8460-5

31. Koundouros N, Poulogiannis G. Reprogramming of fatty acid metabolism in cancer. Br J Cancer **2020**;122:4-22

32. Henne WM, Reese ML, Goodman JM. The assembly of lipid droplets and their roles in challenged cells. EMBO J **2019**;38

33. Listenberger LL, Han X, Lewis SE, Cases S, Farese RV, Jr., Ory DS*, et al.* Triglyceride accumulation protects against fatty acid-induced lipotoxicity. Proc Natl Acad Sci U S A **2003**;100:3077-82

34. Rohrig F, Schulze A. The multifaceted roles of fatty acid synthesis in cancer. Nat Rev Cancer **2016**;16:732-49

35. Basseri S, Austin RC. Endoplasmic reticulum stress and lipid metabolism: mechanisms and therapeutic potential. Biochem Res Int **2012**;2012:841362

36. Cheng X, Geng F, Pan M, Wu X, Zhong Y, Wang C*, et al.* Targeting DGAT1 Ameliorates Glioblastoma by Increasing Fat Catabolism and Oxidative Stress. Cell Metab **2020**;32:229-42 e8

37. Wang G, Xu J, Zhao J, Yin W, Liu D, Chen W*, et al.* Arf1-mediated lipid metabolism sustains cancer cells and its ablation induces anti-tumor immune responses in mice. Nat Commun **2020**;11:220

38. Cao SS, Kaufman RJ. Endoplasmic reticulum stress and oxidative stress in cell fate decision and human disease. Antioxid Redox Signal **2014**;21:396-413

39. Walter P, Ron D. The unfolded protein response: from stress pathway to homeostatic regulation. Science **2011**;334:1081-6

40. Kang R, Tang D, Schapiro NE, Loux T, Livesey KM, Billiar TR*, et al.* The HMGB1/RAGE inflammatory pathway promotes pancreatic tumor growth by regulating mitochondrial bioenergetics. Oncogene **2014**;33:567-77

41. Kant S, Kesarwani P, Prabhu A, Graham SF, Buelow KL, Nakano I*, et al.* Enhanced fatty acid oxidation provides glioblastoma cells metabolic plasticity to accommodate to its dynamic nutrient microenvironment. Cell Death Dis **2020**;11:253

42. Laiakis EC, Strassburg K, Bogumil R, Lai S, Vreeken RJ, Hankemeier T*, et al.* Metabolic phenotyping reveals a lipid mediator response to ionizing radiation. J Proteome Res **2014**;13:4143-54

43. Accioly MT, Pacheco P, Maya-Monteiro CM, Carrossini N, Robbs BK, Oliveira SS*, et al.* Lipid bodies are reservoirs of cyclooxygenase-2 and sites of prostaglandin-E2 synthesis in colon cancer cells. Cancer Res **2008**;68:1732-40

44. Cruz ALS, Barreto EA, Fazolini NPB, Viola JPB, Bozza PT. Lipid droplets: platforms with multiple functions in cancer hallmarks. Cell Death Dis **2020**;11:105

45. Prima V, Kaliberova LN, Kaliberov S, Curiel DT, Kusmartsev S. COX2/mPGES1/PGE2 pathway regulates PD-L1 expression in tumor-associated macrophages and myeloid-derived suppressor cells. Proc Natl Acad Sci U S A **2017**;114:1117-22

46. Finetti F, Travelli C, Ercoli J, Colombo G, Buoso E, Trabalzini L. Prostaglandin E2 and Cancer: Insight into Tumor Progression and Immunity. Biology (Basel) **2020**;9

47. Qiu J, Shi Z, Jiang J. Cyclooxygenase-2 in glioblastoma multiforme. Drug Discov Today **2017**;22:148-56

48. Penas-Prado M, Hess KR, Fisch MJ, Lagrone LW, Groves MD, Levin VA*, et al.* Randomized phase II adjuvant factorial study of dose-dense temozolomide alone and in combination with isotretinoin, celecoxib, and/or thalidomide for glioblastoma. Neuro Oncol **2015**;17:266-73

49. Dilly AK, Honick BD, Lee YJ, Bartlett DL, Choudry HA. Synergistic apoptosis following endoplasmic reticulum stress aggravation in mucinous colon cancer. Orphanet J Rare Dis **2020**;15:211

50. Reardon DA, Brandes AA, Omuro A, Mulholland P, Lim M, Wick A*, et al.* Effect of Nivolumab vs Bevacizumab in Patients With Recurrent Glioblastoma: The CheckMate 143 Phase 3 Randomized Clinical Trial. JAMA Oncol **2020**;6:1003-10

Figure 1

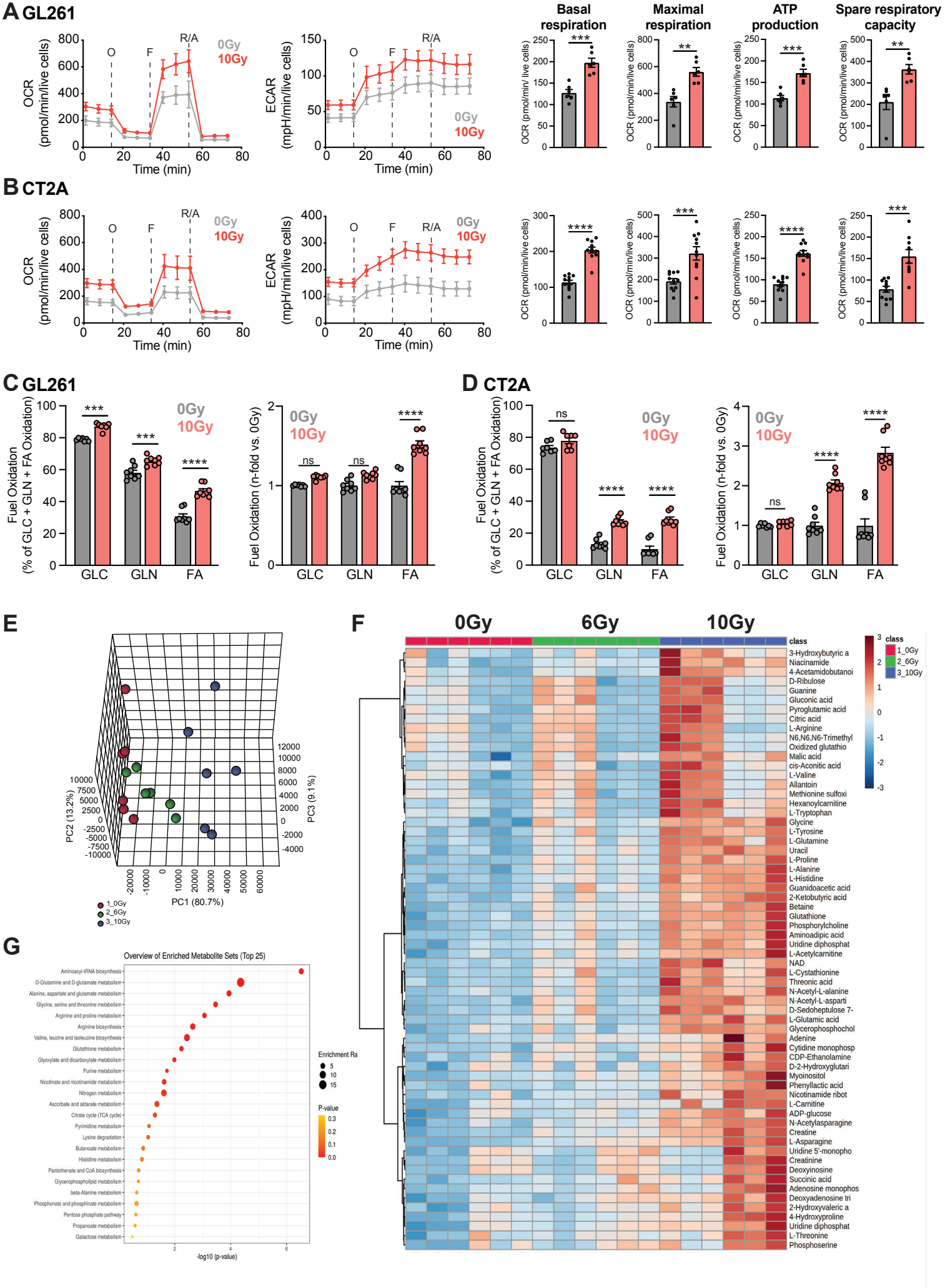
A GL261
OCR (pmol/min/live cells)
ECAR (mpH/min/live cells)
Time (min)
O
F
R/A
0Gy
10Gy
Basal respiration
Maximal respiration
ATP production
Spare respiratory capacity
B CT2A
C GL261
Fuel Oxidation (% of GLC + GLN + FA Oxidation)
Fuel Oxidation (n-fold vs. 0Gy)
GLC
GLN
FA
ns
D CT2A
E
PC1 (80.7%)
PC2 (13.2%)
PC3 (9.1%)
1_0Gy
2_6Gy
3_10Gy
F
0Gy
6Gy
10Gy
class
G
Overview of Enriched Metabolite Sets (Top 25)
Enrichment Ra
P-value
-log10 (p-value)

Figure 2

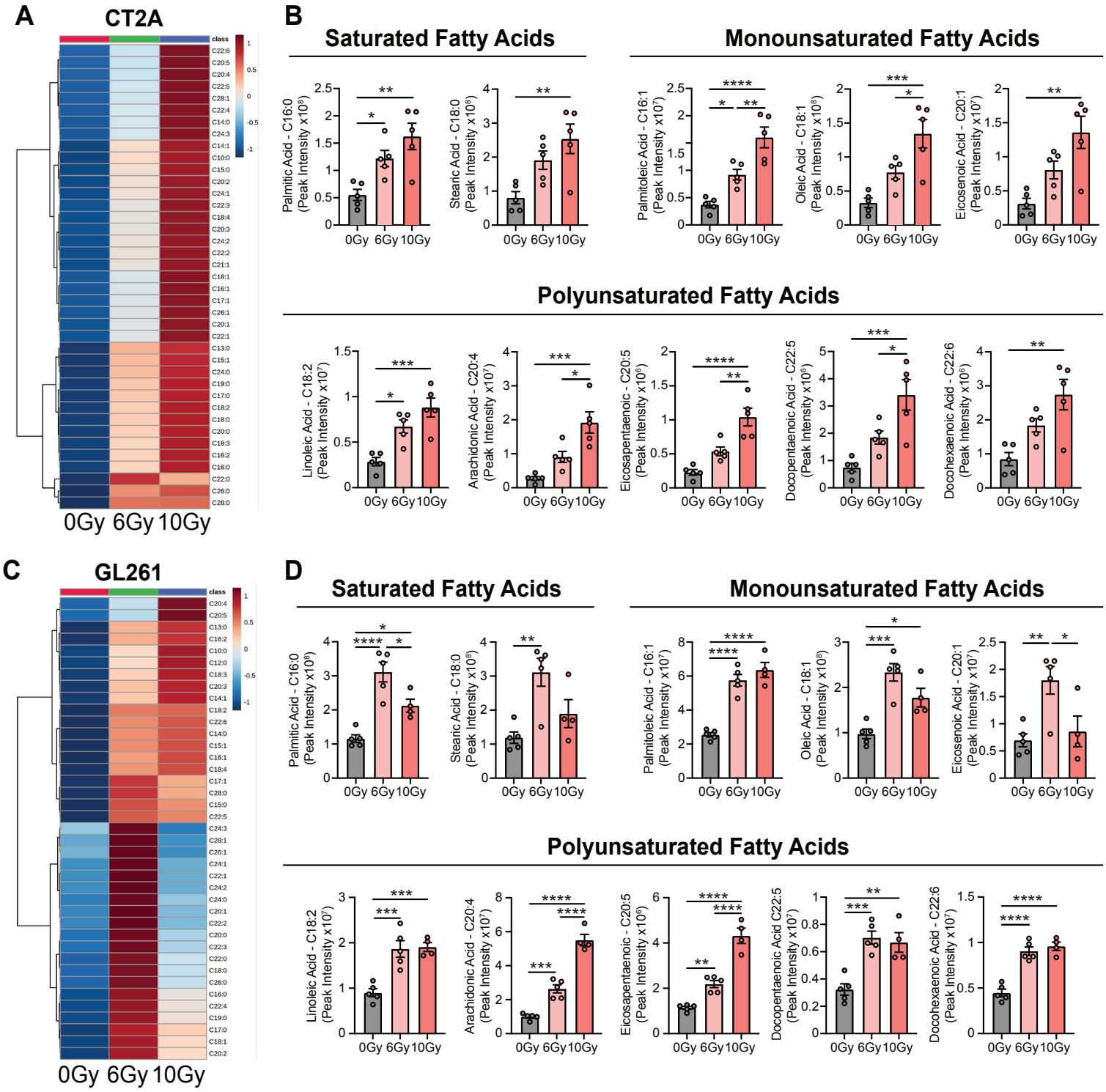
A
CT2A
class
0Gy 6Gy 10Gy
B
Saturated Fatty Acids
Palmitic Acid - C16:0 (Peak Intensity x10^8)
Stearic Acid - C18:0 (Peak Intensity x10^8)
Monounsaturated Fatty Acids
Palmitoleic Acid - C16:1 (Peak Intensity x10^7)
Oleic Acid - C18:1 (Peak Intensity x10^8)
Eicosenoic Acid - C20:1 (Peak Intensity x10^7)
Polyunsaturated Fatty Acids
Linoleic Acid - C18:2 (Peak Intensity x10^7)
Arachidonic Acid - C20:4 (Peak Intensity x10^7)
Eicosapentaenoic - C20:5 (Peak Intensity x10^6)
Docopentaenoic Acid - C22:5 (Peak Intensity x10^6)
Docohexaenoic Acid - C22:6 (Peak Intensity x10^6)
0Gy 6Gy 10Gy
C
GL261
class
0Gy 6Gy 10Gy
D
Saturated Fatty Acids
Palmitic Acid - C16:0 (Peak Intensity x10^8)
Stearic Acid - C18:0 (Peak Intensity x10^8)
Monounsaturated Fatty Acids
Palmitoleic Acid - C16:1 (Peak Intensity x10^7)
Oleic Acid - C18:1 (Peak Intensity x10^8)
Eicosenoic Acid - C20:1 (Peak Intensity x10^7)
Polyunsaturated Fatty Acids
Linoleic Acid - C18:2 (Peak Intensity x10^7)
Arachidonic Acid - C20:4 (Peak Intensity x10^7)
Eicosapentaenoic - C20:5 (Peak Intensity x10^6)
Docopentaenoic Acid C22:5 (Peak Intensity x10^7)
Docohexaenoic Acid - C22:6 (Peak Intensity x10^7)
0Gy 6Gy 10Gy

Figure 3

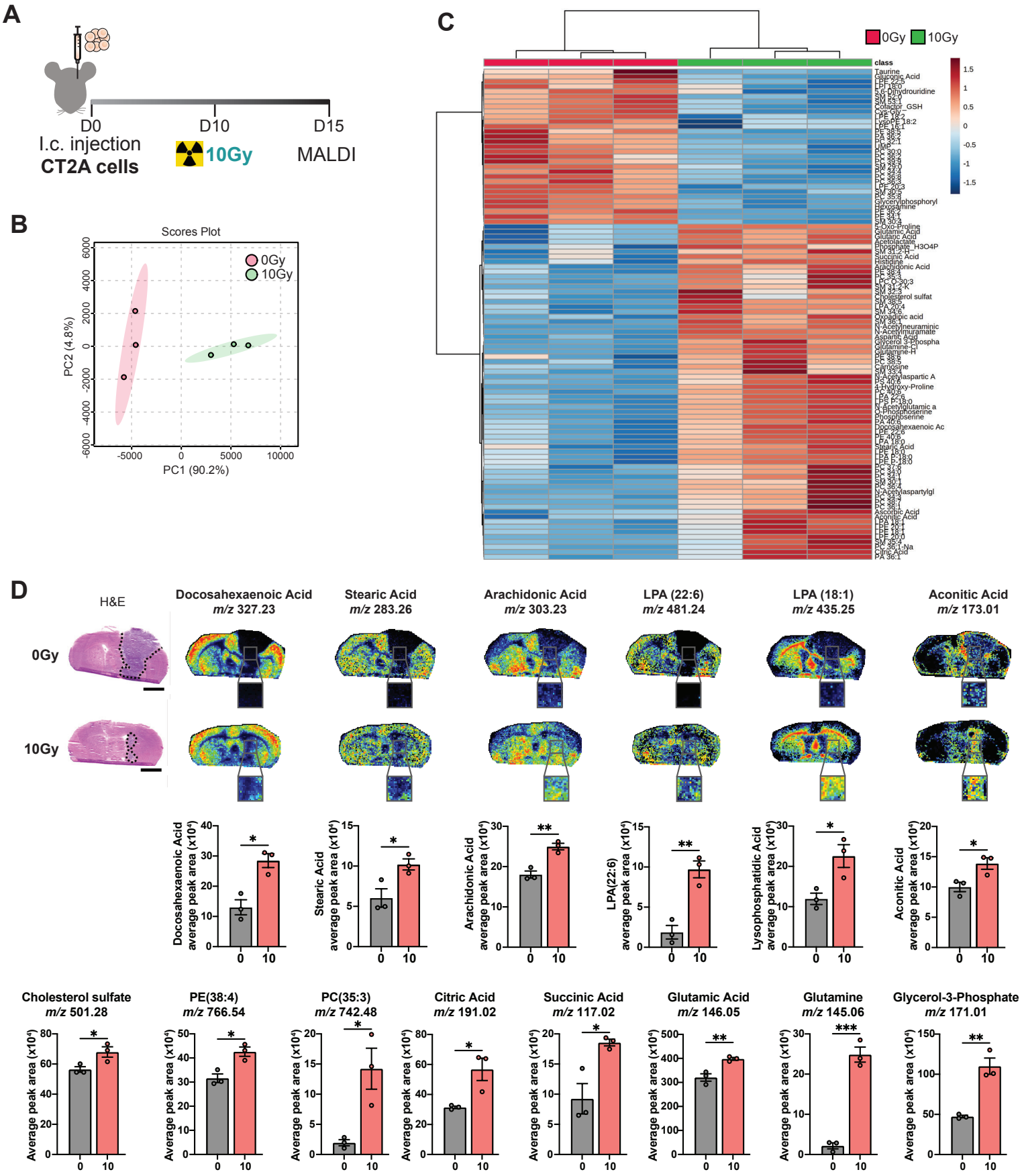
A
D0
D10
D15
I.c. injection
CT2A cells
10Gy
MALDI
B
Scores Plot
0Gy
10Gy
PC2 (4.8%)
PC1 (90.2%)
C
0Gy
10Gy
class
D
H&E
0Gy
10Gy
Docosahexaenoic Acid
m/z 327.23
Stearic Acid
m/z 283.26
Arachidonic Acid
m/z 303.23
LPA (22:6)
m/z 481.24
LPA (18:1)
m/z 435.25
Aconitic Acid
m/z 173.01
Docosahexaenoic Acid average peak area (x10⁴)
Stearic Acid average peak area (x10⁴)
Arachidonic Acid average peak area (x10⁴)
LPA(22:6) average peak area (x10⁴)
Lysophosphatidic Acid average peak area (x10⁴)
Aconitic Acid average peak area (x10⁴)
Cholesterol sulfate
m/z 501.28
PE(38:4)
m/z 766.54
PC(35:3)
m/z 742.48
Citric Acid
m/z 191.02
Succinic Acid
m/z 117.02
Glutamic Acid
m/z 146.05
Glutamine
m/z 145.06
Glycerol-3-Phosphate
m/z 171.01
Average peak area (x10⁴)

Figure 4

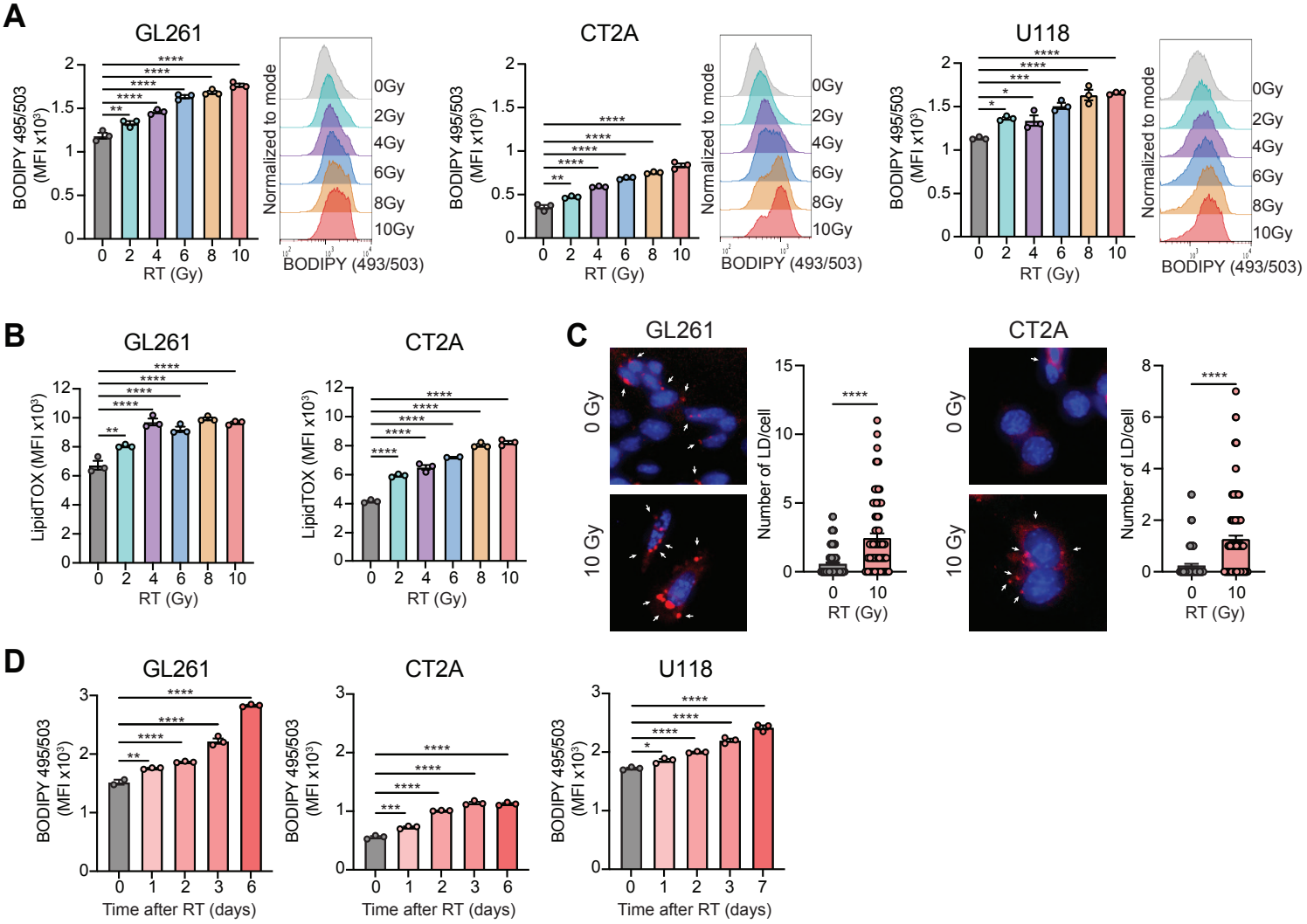
A
GL261
CT2A
U118
BODIPY 495/503 (MFI x10³)
RT (Gy)
Normalized to mode
BODIPY (493/503)
0Gy
2Gy
4Gy
6Gy
8Gy
10Gy
B
LipidTOX (MFI x10³)
C
0 Gy
10 Gy
Number of LD/cell
D
Time after RT (days)

Figure 5

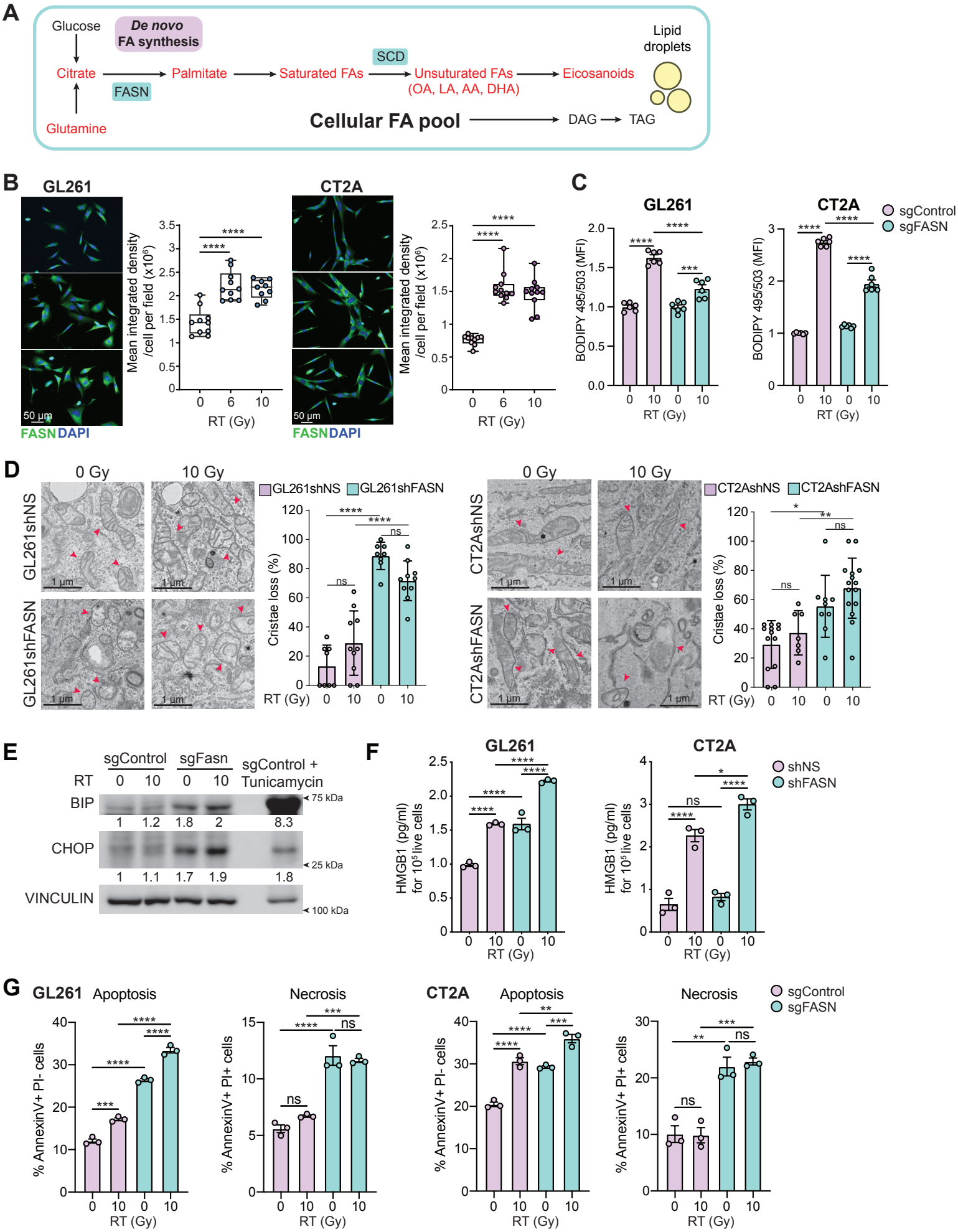
A
Glucose
De novo FA synthesis
Citrate
FASN
Palmitate
Saturated FAs
SCD
Unsuturated FAs (OA, LA, AA, DHA)
Eicosanoids
Lipid droplets
Glutamine
Cellular FA pool
DAG
TAG
B
GL261
CT2A
Mean integrated density /cell per field (x10^6)
RT (Gy)
50 µm
FASN DAPI
C
GL261
CT2A
BODIPY 495/503 (MFI)
sgControl
sgFASN
RT (Gy)
D
0 Gy
10 Gy
GL261shNS
GL261shFASN
GL261shNS
GL261shFASN
Cristae loss (%)
RT (Gy)
1 µm
CT2AshNS
CT2AshFASN
CT2AshNS
CT2AshFASN
E
sgControl
sgFasn
sgControl + Tunicamycin
RT
BIP
CHOP
VINCULIN
75 kDa
25 kDa
100 kDa
F
GL261
CT2A
HMGB1 (pg/ml) for 10^5 live cells
shNS
shFASN
RT (Gy)
G
GL261
CT2A
Apoptosis
Necrosis
% AnnexinV+ PI- cells
% AnnexinV+ PI+ cells
sgControl
sgFASN
RT (Gy)

Figure 6

A

PRKACB
SMARCD3
PTGES2
ECHS1
SLC27A2
SCD5
PTGES
ACAA1
BCHE
ABCA1
AGPAT2
GGT5
ORMDL2
FASN
HPGD
SCD
ACSS3
AKR1C2
-log10(Adj p-value)
logFC(Recurrent/Primary)

B

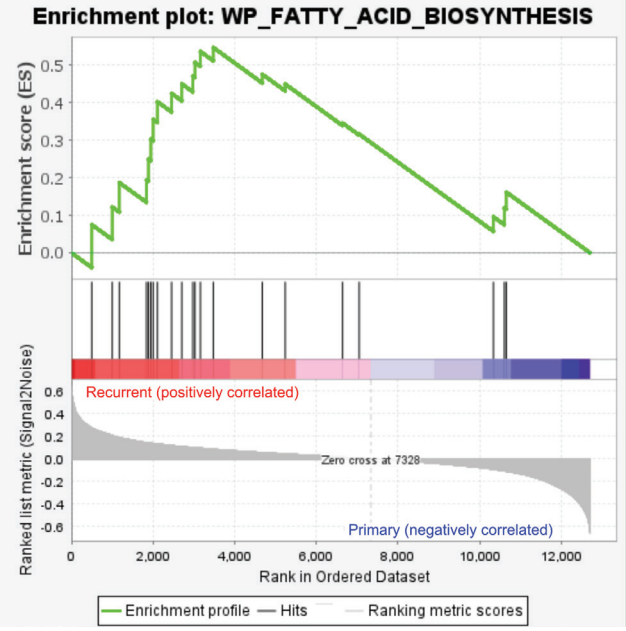
Enrichment plot: WP_FATTY_ACID_BIOSYNTHESIS
Enrichment score (ES)
Recurrent (positively correlated)
Zero cross at 7328
Primary (negatively correlated)
Ranked list metric (Signal2Noise)
Rank in Ordered Dataset
Enrichment profile
Hits
Ranking metric scores